Astron. Astrophys. 324, 196–202 (1997)

ASTRONOMY
AND
ASTROPHYSICS

The Ca I 4227 line as a chromospheric diagnostic for M dwarfs

C.I. Short, J.G. Doyle, and P.B. Byrne

Armagh Observatory, College Hill, Armagh BT61 9DG, N. Ireland (cis@star.arm.ac.uk; jgd@star.arm.ac.uk)

Received 15 October 1996 / Accepted 29 January 1997

Abstract. In M dwarfs the Ca I 4227 line is saturated, therefore, the line core forms at a relatively small column mass density. As a result, the line is a potential diagnostic of chromospheric structure in these stars. We have calculated line profiles out of LTE for a grid of early M dwarf atmospheric models that spans the range from low to high chromospheric pressure and covers a range of observed activity levels. We have found that this line is sensitive to the detailed structure of the chromosphere in the same way as well studied strong lines such as Hα and Ca II HK: as the chromospheric pressure increases, the line changes from absorption to strong emission with a central double reversal. Therefore, observations of the Ca I 4227 line in M dwarfs would provide a useful additional constraint on the structure of the outer atmosphere. We also calculate consistently the line blanketing in the upper atmosphere of models with a chromosphere and transition region and investigate the effect of its inclusion on Ca I 4227. Finally, we demonstrate that the effects of Partial Frequency Redistribution must be taken into account if the Ca I 4227 is to be used as an accurate diagnostic of the $T_{\rm min}$ region in dMe stars.

Key words: stars: late-type – stars: activity – stars: chromospheres – line: formation

1. Introduction

One of the main outstanding problems in stellar astrophysics is the nature of the non-radiative heating that gives rise to the chromospheric and coronal temperature inversion in late-type stars. In order to constrain heating theories it is necessary to have accurate and detailed semi-empirical models of the outer atmospheres of these stars. Strong resonant absorption lines such as the H I Lyman α, Ca II HK, and Mg II hk lines have been the main chromospheric and transition region diagnostics because their cores form at relatively small column mass densities and, therefore, carry information about the gas above $T_{\rm min}$ (for a review see Avrett (1990)). Also, late-type dwarfs can exhibit high levels of transient chromospheric activity, such as flares, and the cores of strong lines have been used to model the flaring state of the plasma (for a review see, Haisch et al. 1991).

In order to further constrain chromospheric models, it is necessary to develop additional spectral diagnostics for which the formation depends on the chromospheric structure in a way that differs somewhat from that of previous diagnostics, and, therefore, provide diagnostic complements. Also, because the Ca II HK and Mg II hk lines are either far out on the Wien side of the emergent flux distribution where the star is faint, or not accessible from the ground, it is desirable to find other diagnostics that are more observable. For example, Andretta et al. (1996) (henceforth ADB) have performed a theoretical investigation of the Na I D lines in a grid of chromospheric models corresponding to an early M star with a range of chromospheric activity levels. They show that the Na I D lines provide a useful diagnostic for semi-empirical chromospheric models. The purpose of this investigation is to study the behavior of the Ca I 4227 line and assess its utility as a chromospheric diagnostic. Recently Ca I 4227 has been used by Mauas & Falchi (1996) to track the time development of a flare on the dMe star AD Leo, and is already known to be responsive to the high activity state of flaring plasma.

In general, the cores of strong lines that form at relatively low gas densities high in the atmosphere differ greatly from those predicted by calculations done with the approximation of Local Thermodynamic Equilibrium (LTE) (see the review by Avrett 1990). The line under investigation may depend on radiative rates in other transitions of the atom, and these rates may be sensitive to the non-local radiation field. Therefore, a detailed description of the background radiation field may be important for an accurate solution of the non-LTE problem (see, for example, Mihalas (1978)). Many previous investigations of chromospheric line formation have either ignored line blanketing in the background radiation field, or, as in the case of ADB, have only included photospheric line blanketing. The multi-line chromospheric modelling of g Her (M6 III) by Luttermoser et al. 1994, which included Ca I 4227, included background line opacities. However, it is unclear if this line opacity corresponds to a photospheric or a chromospheric model, and, in any case, they do not compare the calculated line with and without the inclusion of line blanketing. Because strong lines form well above $T_{\rm min}$, they may be affected by line blanketing that arises

Send offprint requests to: C.I. Short

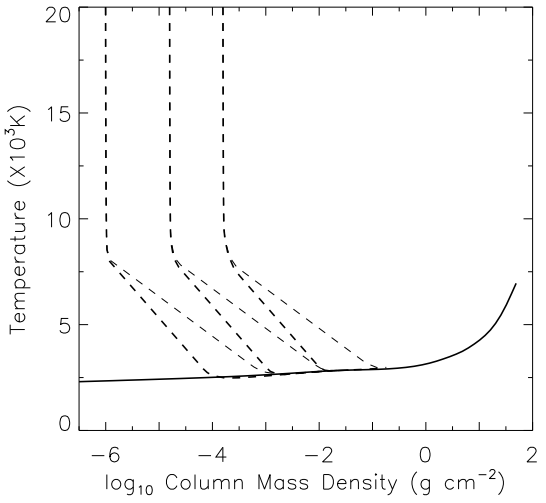

Fig. 1. Temperature structure of models in grid. $1A$ series: thin dashed line, $2A$ series: thick dashed line.

Table 1. Parameters of grid models

	Series $1A$		Series $2A$	
log $m_{\rm o}$	$T_{\rm min}$	log $m_{\rm min}$	$T_{\rm min}$	log $m_{\rm min}$
-6.0	2660	-2.72	2480	-3.72
-4.8	2830	-1.70	2650	-2.70
-3.8	2960	-0.80	2810	-1.80

in the chromosphere and transition region as well as blanketing in the photosphere. Short & Doyle (1996) have used the recently developed PHOENIX model atmosphere code of Allard & Hauschildt (1995) to compute the line opacity in a grid of M dwarf models that take into account the chromospheric and transition region temperature structure. We include this blanketing opacity in our calculations and investigate its effect on the predicted behavior of Ca I 4227.

2. Modelling

2.1. Atmospheric models

Because the calculation of line blanketing opacity is very CPU intensive, we restrict our attention to a sample of six chromospheric models taken from the grid presented by ADB. These models have as their photospheric base a radiative equilibrium model calculated with PHOENIX (Allard & Hauschildt 1995). This photospheric model corresponds to a star of $T_{\rm eff}$ = 3700 K, log g = 4.7, $[\frac{A}{H}]$ = 0.0, and $\xi_{\rm T}$ = 1.0 km s^{-1}. These parameters correspond to a star of spectral type dM0 or dM1 (Lang 1992; Mihalas & Binney 1981). The PHOENIX model atmosphere code includes many important diatomic and triatomic molecules such as TiO and H_2O in the equation of state and opacity and provides realistic models of early M stars (Allard & Hauschildt 1995).

From each of the two model series of ADB labeled $1A$ and $2A$ we take models with the smallest, largest, and an intermediate value of $m_{\rm o}$, which is the mass loading at the onset of the transition region. These two model series differ in the value of $\frac{dT}{d\log m}$ in the chromosphere, with the series $2A$ models having a steeper chromospheric temperature rise. Therefore, comparison of spectral diagnostics computed with these two model series allows an assessment of the sensitivity to the steepness of the chromospheric gradient (or, equivalently, the thickness of the chromosphere) and the location of $T_{\rm min}$. The constancy of the chromospheric $\frac{dT}{d\log m}$ in these models is in keeping with the results of previous semi-empirical modeling of the outer atmospheres of a large variety of late-type stars (cf. Eriksson et al. 1983; Basri et al. 1981; Kelch et al. 1979 and other papers in those series). The value of $\frac{dT}{d\log m}$ in the transition region is also constant in these models, and we have chosen to use the sub-set of the grid that has $(\frac{dT}{d\log m})_{\rm TR} = -6.5$. The temperature at the top of the chromosphere where the transition region begins, $T(m_{\rm o})$, is fixed at 8500 K following Houdebine & Doyle (1994). We only consider models that are in radiative equilibrium below $T_{\rm min}$. Therefore, by fixing the value of $T_{\rm min}$ we also fix the value of $m_{\rm min}$, which is the mass loading at $T_{\rm min}$. Table 1 shows the chromospheric parameters of the grid models, and Fig. 1 shows their temperature structure.

The increase in temperature throughout the chromosphere has an associated increase in the micro-turbulent velocity, $\xi_{\rm T}$. In these models, $\xi_{\rm T}$ rises exponentially with decreasing log(m) in the chromosphere to a value of $\approx$ 10 km s^{-1} at $m_{\rm o}$, then rises rapidly in the transition region to a value of $\approx$ 50 km s^{-1}. A value of 10 km s^{-1} at the top of the chromosphere is typical of values found for other late-type stars (see, for example, Eriksson et al. (1983) and papers in that series).

2.2. Line opacity

Short & Doyle (1996) have used PHOENIX to compute for this grid of models the mean of the total mass absorption due to lines, $\kappa_{\rm l}$, in $2A$ intervals from 500 to 50000A. The line lists used for the calculation include $\approx$ 70 million atomic and molecular lines. They compute $\kappa_{\rm l}$ at all depths from the base of the photosphere to a point in the lower transition region around a temperature of 20 000 K. Short & Doyle (1996) contains a more detailed discussion of how $\kappa_{\rm l}$ was computed and a description of how $\kappa_{\rm l}$ behaves in the chromosphere and transition region.

2.3. Hydrogen

Before calculating Calcium line profiles, we first re-evaluate the Hydrogen ionization equilibrium in our models by using the code MULTI (Carlsson 1986) to solve the combined radiative transfer and statistical equilibrium equations for an atomic model that incorporates the lowest nine levels of H I and the H II state. In the upper chromosphere and lower transition region, H I contributes significantly to $N_{\rm e}$, therefore, the density structure at these heights is partially determined by the HI/II ionization balance. Therefore, we iterate the non-LTE solution

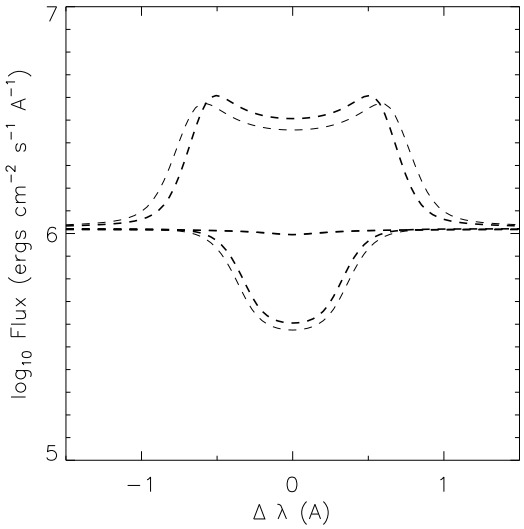

Fig. 2. Hα flux profiles for the $1A$ series (thin line) and the $2A$ series (thick line). The lowest pressure model is the one that has the weakest line absorption.

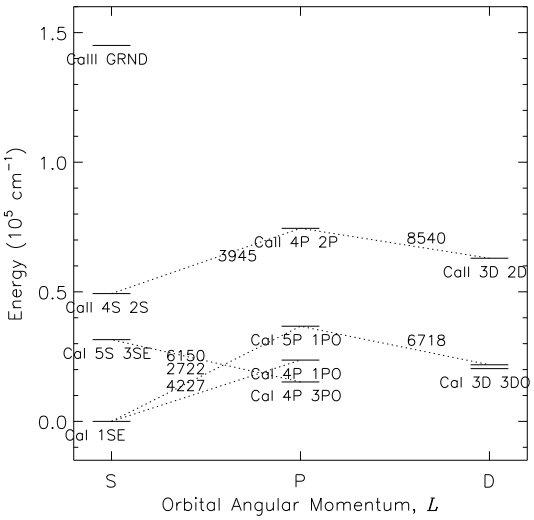

Fig. 3. Grotrian diagram showing the eleven terms and six multiplets of the 14-level Ca I/II/III model atom.

and the equation of hydrostatic equilibrium to convergence. The radiative transfer problem is solved in detail for all 36 $b-b$ transitions connecting the nine H I states and for the $b-f$ transitions of these states. The Lyα line, which has a significant effect on the statistical equilibrium of hydrogen, is treated as a pure Doppler core to approximate the effect of Partial Frequency Distribution (PRD) (Lites et al. 1987). The calculation of the background radiation field includes the addition of the PHOENIX line opacities, $\kappa_{\rm l}$, to the continuous opacities normally computed by MULTI. See Short & Doyle (1996) for a detailed study of how the Hydrogen spectrum and the equilibrium $N_{\rm e}$ structure is affected by the inclusion of background line opacity.

As a by-product of the Hydrogen ionization equilibrium calculation, we obtain synthetic Hα profiles. The morphology of Hα has been the principle diagnostic for classifying dM stars by activity level. Therefore, for reference, we show in Fig. 2 the computed Hα profiles for the model grid. This figure demonstrates that our grid spans the range of observed activity level from quiescent dM stars with weak Hα absorption, to moderately active dM stars with strong Hα absorption, to the most active dMe stars with strong Hα emission.

2.4. Calcium

The ground state ionization energies of Ca I and Ca II are 6.11 eV and 17.98 ev, respectively. As a result, Ca II forms the reservoir population throughout most of the photosphere and chromosphere, except for the transition region where the reservoir shifts to Ca III and the $T_{\rm min}$ region where the ionization equilibrium is almost evenly balanced between Ca I and Ca II. Therefore, the Ca I population is expected to be sensitive to detailed rates in transitions connecting Ca I and Ca II in the region where Ca I 4227 forms. Therefore, a careful non-LTE treatment that includes both ionization stages is particularly important for an accurate result.

We use MULTI to solve simultaneously the coupled radiative transfer and statistical equilibrium equations for an atomic model that incorporates eight states of Ca I, five states of Ca II, and the ground state of Ca III. Ten $b-b$ and thirteen $b-f$ transitions are treated in detail. Fig. 3 shows a Grotrian diagram that identifies the included states and $b-b$ transitions. For clarity the diagram shows only terms and multiplets rather than the individual levels and lines treated in the calculation. The Ca I 4227 line is a singlet transition that connects the $4S^2\ ^1S$ ground state to the $4P\ ^1P_O$ state. Collisional excitations and ionizations among all levels due to electrons are included. All atomic data are those compiled and presented by Drake (1991), which we have found to provide a very close fit to the observed solar Ca I 4227 profile. The Ca calculation incorporates the non-LTE $N_{\rm e}$ structure produced by the H I/II calculation.

We include the PHOENIX $\kappa_{\rm l}$ opacities of Short & Doyle (1996) in all the $b-f$ transitions and in the Ca I 4227 and Ca II HK b-b transitions after removal of the Ca opacity from $\kappa_{\rm l}$. These were incorporated using a modified version of MULTI that was presented in ADB. For the $b-b$ transitions, $\kappa_{\rm l}$ was included as a straight arithmetic mean in $2A$ intervals. For the $b-f$ transitions $\kappa_{\rm l}$ was included as a harmonic mean in $100A$ intervals. An interval width of $100A$ is necessary because normally a sparse frequency sampling of the $b-f$ continua is used in MULTI calculations in order to control the computation time. A harmonic mean was used because occasional strong lines have a disproportionately large effect on the straight mean in a large wavelength interval.

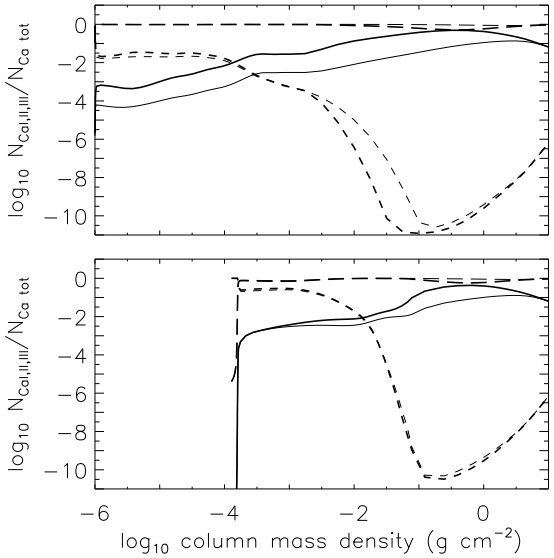

Fig. 4. Population density of Ca I (solid line), Ca II (long dashed line), and Ca III (short dashed line) relative to the total Ca population. Thin lines: continuous background opacity only; thick lines: $\kappa_{\rm l}$ included in background opacity. The top and bottom panels show the lowest and highest pressure models in the $1A$ series, respectively.

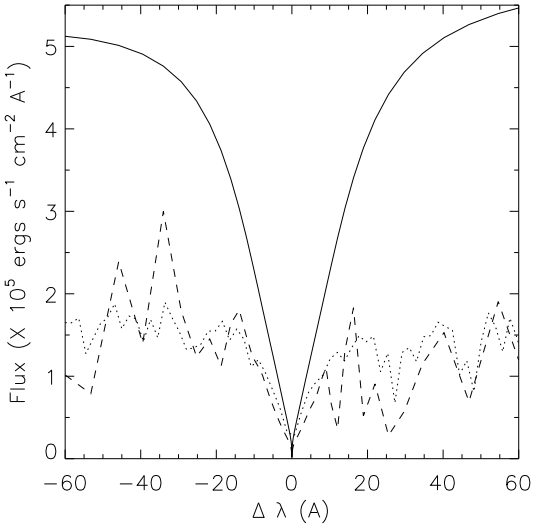

Fig. 5. Ca I 4227 line for lowest pressure model in $1A$ series with and without line blanketing included in background opacity (dashed and solid line, respectively), and the observed spectrum (dotted line).

3. Results and discussion

3.1. The effect of line blanketing

Fig. 4 shows the non-LTE population of Ca I, Ca II, and Ca III as a fraction of the total Ca population for the lowest and highest pressure models in the $1A$ series with and without inclusion of $\kappa_{\rm l}$. For reference, the ground state photoionization energies of Ca I and Ca II correspond to 203 and 104 nm, respectively. In the lowest pressure model the Ca I population is *increased* by approximately an order of magnitude throughout the upper photosphere and entire chromosphere and the Ca III population is *decreased* by almost two orders of magnitude just above $T_{\rm min}$ by the inclusion of $\kappa_{\rm l}$. This is consistent with the reduction of photoionizing flux that is expected to occur because of the additional opacity. The Ca II stage forms the population reservoir throughout most of the atmosphere, therefore, it is much less affected by the amount of opacity. Nevertheless, the Ca II population is slightly reduced by the inclusion of $\kappa_{\rm l}$ in the $T_{\rm min}$ region where locally the Ca I and Ca II populations are almost equal.

The effect of $\kappa_{\rm l}$ on the Ca I population in the highest pressure model is similar to that in the lowest pressure model, although the effect is localized to the upper photosphere and $T_{\rm min}$ region. Fig. 4 demonstrates that the inclusion of $\kappa_{\rm l}$ is necessary for an accurate calculation of the Ca I 4227 line profiles because the Ca I population is sensitive to the treatment of the background opacity.

The dashed and solid lines in Fig. 5 show, respectively, the entire Ca I 4227 line profile with and without line blanketing included in the background opacities. The background opacity depresses the wings by more than a factor of two in many places and must be taken into account when computed line profiles are compared to observed profiles. Normally, a computed flux spectrum is divided by the computed background continuum flux and compared to an observed spectrum that has been rectified to a continuum flux of unity. However, in this case, the computed background flux is line blanketed. Furthermore, for stars of this type, this spectral region is completely blanketed. As a result, we do not know what the background continuum flux is for our models. Therefore, it is not straightforward to normalize the computed spectra to a continuum level of unity; in fact, to do so would require using the same techniques that are used to rectify an observed spectrum. Therefore, in the following analysis we study computed line profiles in absolute flux units and scale observed spectra to the computed pseudo-continuum.

The dotted line in Fig. 5 shows a moderate resolution observed spectrum taken by one of us (Doyle) of Gliese 156.1 (V = 10.86, dM1.5, Gliese 1969). The spectrum has been degraded to a sampling of $2A$ by integration with a boxcar function to match the resolution of the line opacity in the calculated line profile. The observed spectrum has been arbitrarily scaled in flux so that the pseudo-continua are in general agreement. There is some qualitative agreement in the detailed shape of the spectra on the red side of the line, but not on the blue side. Luttermoser et al. (1994) found the same result in their attempt to fit the Ca I 4227 line in the spectrum of g Her (M6 III). We speculate that there may be a local region of particularly severe inaccuracy in the atomic line list data just to the blue of $4227A$. Nevertheless, the overall fit shown in Fig. 5 gives us confidence that our treatment of background line opacity is qualitatively correct.

3.2. Response to chromospheric structure

The thin and thick dashed lines in Fig. 6 show the computed Ca I 4227 line profile for the series $1A$ and $2A$ models, respectively. The profile with the strongest absorption corresponds to

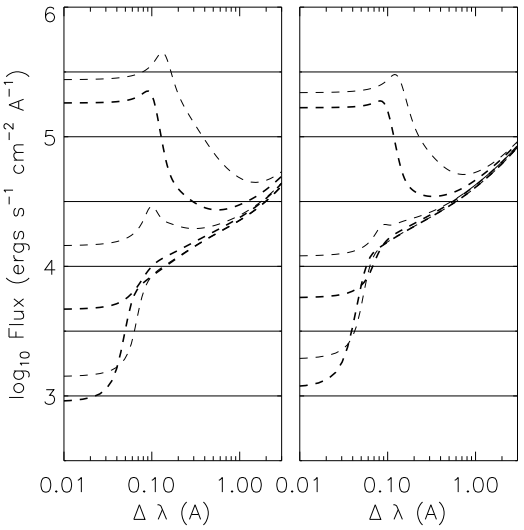

Fig. 6. Ca I 4227 line core for models of series $1A$ (thin lines) and $2A$ (thick lines). Left panel: line blanketing; right panel: no line blanketing.

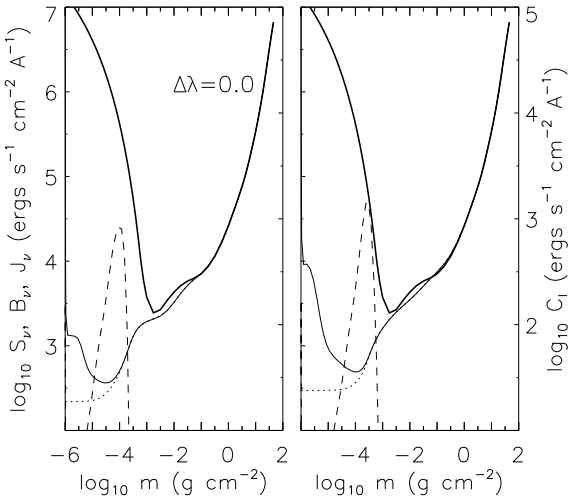

Fig. 7. Ca I 4227 total monochromatic intensity source function, S_ν (thin solid line) and contribution function, $C_{\rm I}$ (dashed line) at $\Delta\lambda$ = 0.0 and μ = 0.887 for *lowest* pressure model in $1A$ series. Also shown is the Planck function, B_ν (thick solid line), and the mean intensity, J_ν (dotted line). Left panel: line blanketing; right panel: no line blanketing.

the lowest pressure model and that with the strongest emission corresponds to the highest pressure model. The left panel shows profiles calculated with the inclusion of $\kappa_{\rm l}$ in the background opacities, and the right panels show profiles without the inclusion of $\kappa_{\rm l}$. Comparison among the series $1A$ profiles shows that the line core is very sensitive to the mass loading at $m_{\rm o}$ and, therefore, the chromospheric pressure. Comparison of the left and right panels shows that in some cases the inclusion of $\kappa_{\rm l}$ in the background opacities makes a significant difference to the line profiles. In particular, for the highest pressure models the difference between the line profile with and without the inclusion of $\kappa_{\rm l}$ is of the same order as the difference between the series $1A$ and $2A$ models. Therefore, it is necessary to include $\kappa_{\rm l}$ in order to use this line as an accurate diagnostic.

Fig. 7 shows for the lowest pressure model in the $1A$ series the total monochromatic intensity source function, S_ν, of the computed Ca I 4227 line at line center ($\Delta\lambda$ = 0.0) at an angle near disk center (μ = 0.887). The Planck function, B_ν, and the mean intensity, J_ν, are also shown for reference. Also shown is the intensity contribution function, $C_{\rm I}$. The left panel shows the case where $\kappa_{\rm l}$ has been included in the background radiation field, and the right panel shows the case where $\kappa_{\rm l}$ is not included.

For the lowest pressure model, S_ν at $\Delta\lambda$ = 0.0 is monotonically decreasing throughout most of the chromosphere, and only starts to increase again under the influence of the transition region at depths well above those where $C_{\rm I}$ peaks. Therefore, the emergent line profile is purely in absorption. Comparison of the left and right panels shows that the inclusion of $\kappa_{\rm l}$ in the background radiation field lowers S_ν slightly and causes the peak of $C_{\rm I}$ to move outward to lower values of S_ν, thus lowering the emergent I_ν in the line core.

Fig. 8 shows the same quantities for the highest pressure model in the $1A$ series at three critical wavelengths: line center ($\Delta\lambda$ = 0.0), near the peak emission of the central double reversal ($\Delta\lambda$ = 0.1), and in the inner wing near the emission minimum ($\Delta\lambda$ = 1.0).

This figure demonstrates that the central double reversal of the emergent line profile is due to the same mechanism that leads to similar behavior in the much studied Ca II HK lines. Because of the higher density of this model $S_\nu \approx B_\nu$ until well above $T_{\rm min}$ before declining in value in the upper chromosphere. This leads to a "S_ν hump" in the chromosphere. At $\Delta\lambda$ = 0.0, $C_{\rm I}$ peaks near a local minimum in S_ν above the hump and below the depth where S_ν increases again due to the transition region. At $\Delta\lambda$ = 0.1, $C_{\rm I}$ peaks closer to the local S_ν maximum in the hump, thus leading to the central double reversal in the emergent I_ν profile. As in the case of the Ca II HK lines, at values of $\Delta\lambda$ where $C_{\rm I}$ peaks near $T_{\rm min}$ ($1.0A$ in this case) there is a minimum in the I_ν profile that may be used as a powerful diagnostic of $T_{\rm min}$ because S_ν is strongly coupled to B_ν near $T_{\rm min}$.

Comparison of the left and right panels in Fig. 8 shows that inclusion of $\kappa_{\rm l}$ raises S_ν at $\Delta\lambda$ = 0.1 in the upper chromosphere leading to a larger I_ν in the emission peak. Also, S_ν at $\Delta\lambda$ = 1.0 in the vicinity of $T_{\rm min}$ decreases slightly and $C_{\rm I}$ is pushed outward leading to a lower emission minimum in I_ν. These changes due to $\kappa_{\rm l}$ are clearly visible in Fig. 6. Therefore, inclusion of line blanketing in the Ca I/II/III transitions is necessary in order to use this line as an accurate diagnostic of chromospheric structure.

3.3. PRD effects

The line profiles described above were calculated with the assumption of Complete Frequency Redistribution. However, it is known that strong resonance lines such as Hα and Ca II HK are significantly affected by Partial Frequency Redistribution (PRD) effects in late-type stellar atmospheres (see Linsky 1985

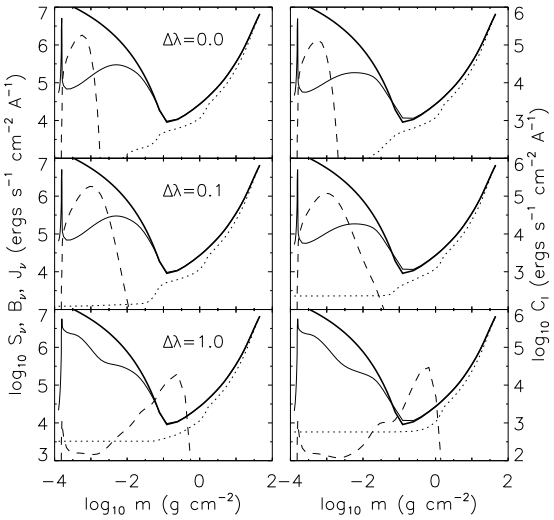

Fig. 8. Ca I 4227 total monochromatic intensity source function, S_ν (thin solid line) and contribution function, $C_{\rm I}$ (dashed line) at μ = 0.887, B_ν (thick solid line), and J_ν (dotted line) for *highest* pressure model in $1A$ series at three wavelengths. Left panel: line blanketing; right panel: no line blanketing.

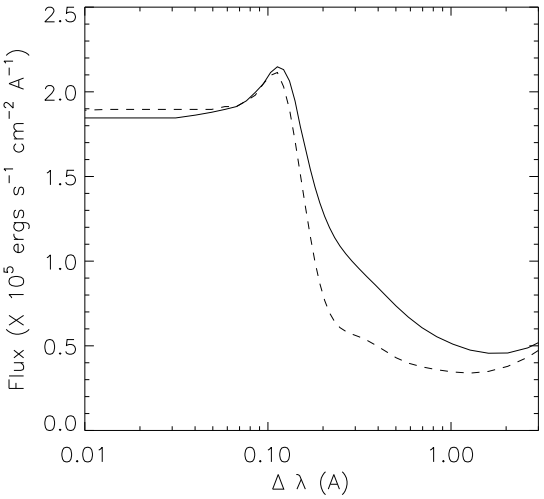

Fig. 9. Ca I 4227 calculated with CRD (solid line) and PRD (dashed line) for the highest pressure model in the $1A$ series.

for a review). In their multi-line modelling of g Her, Luttermoser et al. (1994) included PRD effects in their calculation of Ca I 4227. However, because this line does not show an emission reversal in spectra of g Her, they do not present a discussion of the effect of PRD on the calculated line.

We have used a version of MULTI that has been modified to include the effects of PRD (Uitenbroek 1989) to re-calculate the Ca I 4227 line in the highest pressure model of the $1A$ series, for which the line core is most strongly reversed. Fig. 9 shows a comparison of the CRD and PRD profiles. The flux at line center and in the emission peaks are negligibly affected by PRD. However, the minimum flux is reduced in the PRD case by $\lesssim$ 10%. This reduction in the flux minimum is similar to what has been found for the well-studied Ca II K line, and is a well understood effect of PRD (see Uitenbroek 1989, for example). From the discussion above, we have determined that the flux minimum is an indicator of the value and location of $T_{\rm min}$. Therefore, the results shown in Fig. 9 indicate that PRD must be taken into account if this line is to be used as a semi-empirical diagnostic of the lower chromosphere. Nevertheless, the relative behavior shown in Fig. 6 due to changes in the gross chromospheric structure, chromospheric pressure, and treatment of background opacity, although based on CRD calculations, is still qualitatively correct. Unfortunately, we are unable at this time to include background line opacity in our PRD calculations.

4. Conclusion

We have demonstrated that the Ca I 4227 line is sensitive to the chromospheric structure of dM stars. In particular, as chromospheric pressure increases from that of a quiescent chromosphere to that of a highly active chromosphere, the line changes from being strongly in absorption to being strongly in emission with a central double reversal. In the most active stars, the line source function is strongly coupled to the thermal temperature at, and just above $T_{\rm min}$. Therefore, the doubly reversed emission core of stars with high chromospheric pressure may be used as a "thermometer" for the $T_{\rm min}$ region in the same way that the Ca II HK lines are used. However, the Ca I 4227 line has the advantage of being more observable in M stars than is the Ca II HK line because it is closer to the Wien peak of the emergent flux distribution. Also, as in the case of the Ca II HK lines, the effect of PRD must be taken into account in the line profile calculation if the line is to be used as an accurate diagnostic of $T_{\rm min}$. Unfortunately, there is a lack of observations of this line in dM stars of sufficient resolution and signal-to-noise to fit the core. Observations of this line with $R > 150000$ and $S : N$ in the pseudo-continuum of ≈ 200 for dM stars of a variety of activity levels are needed to exploit the modelling results shown here.

The inclusion of $\kappa_{\rm l}$ affects the Ca I 4227 profile, both by its direct effect on the radiative transfer of the Ca I atom, and by its affect on the chromospheric $N_{\rm e}$ structure that arises from the ionization balance of H I/II. Because the Lyman and Balmer transitions of H I form in the upper atmosphere, it is necessary to include not just photospheric line blanketing in radiation fields forming below $T_{\rm min}$, but also chromospheric and transition region line blanketing in radiation fields that form above $T_{\rm min}$.

Acknowledgements. The main body of this work has been carried out at Armagh Observatory, supported by PPARC grant GR/K04613. We also acknowledge support at Armagh in terms of both software and hardware by the STARLINK Project, funded by the UK PPARC.

We are indebted P. Hauschildt for access to PHOENIX and for extensive help running the code to produce opacity tables. We are also very grateful to Vincenzo Andretta for providing the line blanketed version of Multi and for helpful discussion.

References

Allard, F., & Hauschildt, P. H., 1995, ApJ, 445, 433
Andretta, V., Doyle, J. G., & Byrne, P. B., 1996, A&A, *in press*
Avrett, E. H., 1990, in IAU Symposium 138, Solar Photosphere: Structure, Convection, and Magnetic Fields., ed. J. O. Stenflo (Dordrecht: Kluwer), p. 3
Basri, G. S., Linsky, J. L., & Eriksson, K., 1981, ApJ, 251, 162
Carlsson, M., 1986, Uppsala Observatory Internal Report no. 33
Drake, J. J., 1991, MNRAS, 251, 369
Eriksson, K., Linsky, J. L., & Simon, T., 1983, ApJ, 272, 665
Gliese, W., 1969, Catalogue of Nearby Stars, (Verlag G. Braun: Karlsruhe)
Haisch, B., Strong, K. T., & Rodono, M., 1991, ARA&A, 29, 275
Houdebine, E. R. & Doyle, J. G., 1994, A&A, 289, 169
Kelch, W. L., Linsky, J. L., & Worden, W. P., 1979, ApJ, 229, 700
Lang, K. R., 1992, Astrophysical Data: Planets and Stars, (Springer-Verlag: New York)
Linsky, J. L., 1985, in Progress in Stellar Spectral Line Formation Theory, eds. J. E. Beckman and L. Crivellari, (Dordrecht: Reidel), p.1
Lites, B. W., Skumanich, A., Rees, D. E., Murphy, G. A., & Carlsson, M., 1987, ApJ, 318, 930
Luttermoser, D. G., Johnson, H. R., & Eaton, J., 1994, ApJ 422, 351
Mauas, P. J. D. & Falchi, A., 1996, A&A 310, 245
Mihalas, D., 1978, Stellar Atmospheres, 2nd ed., (W. H. Freeman and Co.)
Mihalas, D. & Binney, J., 1981, Galactic Astronomy, 2nd ed., (W. H. Freeman and Co.)
Short, C. I. & Doyle, J. G., 1996, A&A, in press
Uitenbroek, H., 1989, A&A 213, 360

This article was processed by the author using Springer-Verlag LaTeX A&A style file *L-AA* version 3.